DOI: 10.1021/ma802551v

Macromolecules
ARTICLE

Synthesis and Self-Assembly of Poly-(diethylhexyloxy-*p*-phenylenevinylene)-*b*-poly(methyl methacrylate) Rod−Coil Block Copolymers

Chun-Chih Ho,[†] Yi-Huan Lee,[‡] Chi-An Dai,[‡] Rachel A. Segalman,[§] and Wei-Fang Su*,[†]

[†]*Department of Materials Science and Engineering and* [‡]*Institute of Polymer Science and Engineering, National Taiwan University, Taipei 106, Taiwan, and* [§]*Department of Chemical Engineering, University of California, Berkeley, and Materials Sciences Division, Lawrence Berkeley National Laboratories, Berkeley, California 94720*

Received November 13, 2008; Revised Manuscript Received April 15, 2009

ABSTRACT: A series of poly(diethylhexyloxy-*p*-phenylenevinylene-*b*-methyl methacrylate) (DEH-PPV-*b*-PMMA) polymers with narrow polydispersity (PDI < 1.1) were synthesized using Siegrist polycondensation and anionic polymerizations followed by "click" chemistry. Alkyne-terminated DEH-PPV and azido-terminated PMMA were synthesized first, and then the two functionalized polymers underwent 1,3-cycloaddition reaction to obtain copolymers. Both the conversion of the end-functionalization of the homopolymers and the yield of the "click" reaction were higher than 98% as determined by ^{1}H nuclear magnetic resonance (^{1}H NMR) and gel permeation chromatography (GPC). Transmission electron microscopy (TEM) and small-angle X-ray scattering (SAXS) studies reveal the details of copolymer morphology. The DEH-PPV-*b*-PMMA system presented here has higher block segregation strength than many previously studied rod−coil block copolymers yet still shows experimentally accessible phase transitions with respect to temperature. As a result, this molecule offers new insight into the competition between rod−rod and rod−coil interactions that occurs in the system. The DEH-PPV rods are organized as a monolayer that is inclined with the lamellar normal (smectic C) for the copolymers containing low volume fraction of PMMA coil (< 54%). However, as the coil fraction increases, the strips containing DEH-PPV pack into hexagonal lattice. In contrast to previous work which demonstrated similar morphologies, the sequence of reversible liquid crystalline and microphase phase transitions is altered as a result of the increased block segregation. Upon heating, the low coil fraction copolymers exhibit a series of clear transitions of smectic−lamellar to amorphous−lamellar to disordered structures. In high coil fraction copolymers, the transitions between smectic−hexagonal to amorphous−hexagonal and smectic−hexagonal to disorder structures could not be clearly differentiated. The order-to-disorder temperature (ODT) decreases slowly with increasing coil fraction while the smectic-to-isotropic transition (SI) temperature stays relatively unchanged. The steady SI temperature suggests that the strong rod−rod interaction keeps the liquid crystalline rod in the nanodomain structure regardless of the amount of coil segment in the copolymers.

Introduction

Block copolymers have attracted enormous interests because of their ability to self-assemble into a variety of regular nanostructures.[1,2] These nanostructures, including spherical, hexagonal, bicontinuous gyroid, and lamellar morphologies, encompass many useful mechanical, electrical, and optical properties.[3] While significant work has been performed on classical coil−coil block copolymers, rod−coil block copolymers have received a great deal of recent attention.[4] If the rod segment is a π-conjugated conducting polymer, it exhibits unique electrical and optical properties that are useful for LED and photovoltaic applications.[5−11] Analogous to classical coil−coil block copolymers, the Flory−Huggins (rod−coil) interaction (χ) and the volume fraction of the two blocks are important in determining phase behavior in rod−coil polymers. An additional three parameters are frequently used to describe the interactions in rod−coil block copolymers: the Maier−Saupe (rod−rod) interaction (μ), geometric difference between coil block and rod block, and the competition between μ and χ.[12,13] Therefore, the thermodynamic phase equilibrium of rod−coil copolymer will be unique and complicated.[14]

In order to investigate the phase behaviors and self-assembly mechanisms of rod−coil block copolymers, the preparation of a well-defined block copolymer is crucial. A broad molecular weight distribution, residual homopolymer, and/or reaction byproduct can affect the morphology of the copolymer. Two main synthetic approaches have been developed for rod−coil block copolymers. In a divergent route the rod macroinitiator is prepared and then used to initiate the living polymerization of the coil block.[5,15−19] The choice of monomer in the coil block is limited by reactivity, and the choice of rod block is severely limited by the requirement of chemical stability under the conditions necessary to polymerize the coil. In contrast, the convergent route makes use of end-coupling of the substituents[20−24] via macrotermination, acid−base chemistry, or the "click" chemistry of Huisgen's 1,3-dipolar cycloaddition reaction.[25−27] These reactions can tolerate a variety of functional groups and solvents and produce a high yield (> 95%) block copolymer.[28−33]

Free energy calculations and scaling arguments have been used to predict the self-assembly behavior and arrangement of rod segments in rod−coil block copolymers.[34−38] Landau free energy

*Corresponding author: E-mail: suwf@ntu.edu.tw.

 Published on Web 05/12/2009

calculations including both compositional and orientational order parameters predict a lamellar phase with liquid crystalline transitions for low coil fraction copolymers, whereas nonlamellar phases including hexagonal and spherical phases are predicted for high coil fraction copolymers.[39] The phase boundary is shifted which apparently is due to the geometric asymmetry and the competition between the rod−coil interaction and the rod−rod interaction.[39−41] Self-consistent-field theory (SCFT) has also been used to investigate the phase behavior of the rod−coil block copolymers predicting bilayer and arrowhead phases for strongly segregated copolymers and strip or puck structures for high coil fraction copolymers.[12,13,42−44]

Experimentally, a large number of intriguing phases have been observed, and their experimental thermodynamic behavior is beginning to be elucidated. While lamellar and hexagonal phases have been observed in the peptide-based rod−coil block copolymers,[45−48] poly(hexyl isocyanate) (PHIC)-based systems exhibit more phases including zigzags and arrow heads.[49] When the rod block gains its stiffness from the steric crowding of side-chain liquid crystals (frequently called mesogen-jacketed rods), smectic A-like and perforated lamellar structures are observed.[50,51] Yet other experimental systems are low enough in molecular weight that the coil is fully extended, and in these systems a wide variety of phases including hexagonal strip, cubic puck, and bicontinuous phases are observed.[52−57] When the chains are polymeric in length, but the segregation strength between the rod and coil is weak, the microphase transition temperatures can be experimentally accessed. Much work has been done recently with poly(diethylhexyloxy-*p*-phenylenevinylene) (DEH-PPV)-based systems in which the side chains appear to help moderate interactions.[20−22,58] Lamellar phases are observed when the segregation is weak or when the geometric asymmetry (ν) is low. Nonlamellar phases such as hexagonal and spherical structures have been observed in conditions of high asymmetry[59] or increased segregation strength.[60,61] Recent work has universalized these phase diagrams in terms of rod−rod interaction (μ) and rod−coil interaction (χ) in a weakly segregated system (DEH-PPV-*b*-polyisoprene),[14] though recent work in a more highly segregated system (DEH-PPV-*b*-poly(4-vinylpyridine)) has demonstrated when the rod−coil repulsion is stronger, competition between the rod alignment and rod−coil separation results in intriguing phases not observed in the weak segregation limit.[60,61] Here, we use an intermediate system that retains phase transitions in an accessible temperature range, but in which the competition between rod alignment and rod−coil separation is stronger (competition term $G = \mu/\chi$). Similar to Sary et al., we find a stronger presence of the nonlamellar phases but are now able to place these on a complete phase diagram indicating both microphase and liquid crystalline order−order and order−disorder transitions. In particular, the DEH-PPV-*b*-PMMA copolymer appears to lead to a smaller G value as compared with the weakly segregated DEH-PPV-*b*-PI system on which previous phase diagrams were based.

Experimental Methods

Materials. α,α′-Dibromo-*p*-xylene (Fluka, 98%), lithium chloride (LiCl, Acros, 99%), sodium azide (NaN_3, Acros, 99%), propargyl bromide (80% in toluene, Fluka), zinc (RdH, >99%), 1,8-diazabicyclo[5.4.0]undec-7-ene (DBU, Fluka, 99%), and copper(I) iodide (RdH, 99.5%) were used without further purification. Methyl methacrylate (MMA, Acros, 99%) and 1,1-diphenylethylene (DPE, Acros, 99%) were dried over CaH_2 overnight, followed by freeze−pump−thaw cycles and vacuum-distilled. The reagents were stored under a nitrogen atmosphere at −4 °C. Tetrahydrofuran (THF, J.T. Baker) was purified by refluxing over fresh sodium benzophenone complex (a deep purple color indicated an oxygen- and moisture-free solvent). It was further dried dropwisely with *sec*-butyllithium (*sec*-BuLi, 1.3 M in cyclohexane, Chemetall) immediately before use. N,N-Dimethylformamide (DMF, J.T. Baker) was dried over 4 Å molecular sieves and used within 2 weeks.

Synthesis of Bromine End-Terminated Poly(methyl methcrylate), 1. Anionic polymerization was carried out in an oxygen-free and moisture-free glass reactor under a nitrogen atmosphere. LiCl (1.1 g, 25.87 mmol) was first placed in a Schlenk flask that was was evacuated and flame-dried. THF (250 mL) and DPE (0.55 mL, 3.10 mmol) were introduced through a cannula, and the reaction mixture was cooled to −78 °C. Subsequently, *sec*-BuLi (1.99 mL, 2.59 mmol) was injected to initiate the DPE, and the color of the solution turned to scarlet instantly. After 15 min, MMA (10 mL, 92.90 mmol) was added, and the reaction mixture immediately became colorless. The reaction was allowed to proceed at −78 °C for 30 min to make poly(methyl methacrylate) (PMMA) anion solution. The PMMA anion solution was introduced dropwisely into a α,α′-dibromo-*p*-xylene (6.83 g, 25.9 mmol) solution. Thirty minutes later, the reaction mixture was terminated with methanol. The corresponding polymer was purified over a basic alumina column to remove LiCl and precipitated twice in hexane to produce a white solid, yield 83%. ^{1}H NMR δ: 0.55 (m, 6H, −CH−CH_3, −CH$_2$−CH_3), 0.83 (s, 3(n + 1)H, −C−CH_3), 1.01 (m, 2H, −CH−CH_2−CH$_3$), 1.79 (m, 2(n + 1) H, −C−CH_2−C−), 2.30 (m, H, −CH$_2$−CH−CH$_3$), 2.47, 2.76 (m, 2H, −C−CH_2−Ar−), 3.58 (m, 3H, −O−CH_3), 4.45 (s, 2H, Ar−CH_2−Br), 6.95 (d, 2H, −CH$_2$−Ar−H meta), 7.10−7.25 (m, 12H, Br−CH$_2$−Ar−H, −C−Ar−H).

Synthesis of Azido-Terminated Poly(methyl methcrylate), 2. The bromine end-functionalized poly(methyl methacrylate) (**1**) (8.0 g, 2.20 mmol) was dissolved in DMF (200 mL), followed by adding excess sodium azide (0.72 g, 11.02 mmol). The reaction mixture was stirred overnight at 60 °C. The polymer was purified over a basic alumina column to remove the remaining NaN_3 and salts. The polymer was then precipitated twice in hexane, yielding a white solid, yield 95%. ^{1}H NMR δ: 0.55 (m, 6H, −CH−CH_3, −CH$_2$−CH_3), 0.83 (s, 3 (n + 1)H, −C−CH_3), 1.01 (m, 2H, −CH−CH_2−CH$_3$), 1.79 (m, 2(n + 1)H, −C−CH_2−C−), 2.30 (m, H, −CH$_2$−CH−CH$_3$), 2.47, 2.76 (m, 2H, −C−CH_2−Ar−), 3.58 (m, 3H, −O−CH_3), 4.29 (s, 2H, Ar−CH_2−Br), 6.95 (d, 2H, −CH$_2$−Ar−H meta), 7.10−7.25 (m, 12H, Br−CH$_2$−Ar−H, −C−Ar−H); ν_{max}(film)/cm^{-1}: 482, 703, 749, 810, 827, 841, 911, 967, 987, 1063, 1148, 1190, 1242, 1269, 1386, 1442, 1481, 1730, 2099 (−N_3), 2845, 2950, 2994, 3441, 3554, and 3620.

Synthesis of Alkyne-Terminated Poly(2,5-di(2′-ethylhexyloxy)-1,4-phenylenevinylene), 3. DEH-PPV with aldehyde end-terminated functionality was synthesized by Siegrist polycondensation, as previously described.[22] The DEH-PPV (8 g, 2.14 mmol) and zinc metal (0.56, 8.58 mmol) were then placed in an evacuated Schlenk flask. THF (250 mL) and propargyl bromide, 80 wt % solution in toluene (0.4 mL, 0.51 mmol), were then introduced. The reaction mixture was allowed to proceed at 50 °C for 1 day. The polymer was purified by precipitating twice in methanol, yield 97%. ^{1}H NMR δ: 0.89 (m, 12(n + 1)H, −CH_3), 1.45 (m, 16(n + 1)H, −CH_2−), 1.81 (m, 2(n + 1)H, −CH−), 2.24 (s, 3H, Ar−CH_3), 2.62, 2.81 (m, 2H, −CH−CH_2−CH), 2.90 (s, H, −C−CH), 3.94 (d, 4H-(n + 1), −O−CH_2−), 5.10 (t, H, Ar−CH−CH$_2$), 5.20 (s, H, −CH−OH), 7.20 (s, 2nH, −CH=), 7.53 (s, 2(n + 1)H, Ar−H).

Synthesis of Poly(2,5-di(2′-ethylhexyloxy)-1,4-phenylenevinylene)-*block*-poly(methyl methcrylate) (DEH-PPV-*b*-PMMA) via "Click" Chemistry, 4. The azido-terminated PMMA (**2**) (1.0 equiv), the alkyne-terminated DEH-PPV (**3**) (2.0 equiv), and CuI (0.4 equiv) were first placed in the Schlenk flask. The flask was evacuated and backfilled with dry nitrogen for three times. THF to make 2 wt % of polymer solution was added. DBU (40 equiv) was then introduced, and the reaction

mixture was maintained at 35 °C. The completion of the reaction was monitored by GPC until the intensity of the peak associated with the elution of block copolymer no longer increased in size. The polymer was precipitated twice in hexane to remove the excess homo DEH-PPV and precipitated twice in methanol; yield 93%.

Gel Permeation Chromatography (GPC). The molecular weight and molecular weight distribution of synthesized polymers were measured using a Waters GPC (Breeze system) and THF used as an eluent at 35 °C. The apparatus was equipped with two Waters Styragel columns (HR3 and HR4E), a refractive index detector (Waters 2414), and a dual-wavelength absorbance detector (Waters 2487). The wavelengths were set at 254 and 465 nm. Poly(methyl methacrylate) standards (Polymer Laboratories) were used for the calibration of PMMA. Polystyrene standards (Waters) were used to determine the polydispersity of DEH-PPV and block copolymers. The polystyrene equivalent polydispersity for all polymers was measured to be less than 1.18.

^{1}H Nuclear Magnetic Resonance (^{1}H NMR). NMR spectra were recorded on a Bruker Avance 400 MHz, and $CDCl_3$ was used as solvent. The number-average molecular weight of the DEH-PPV block was estimated by the comparison of signal integration from the aldehyde proton peak at the chain end to the methylene proton peak neighboring oxygen group on the side chain.

Fourier-Transform Infrared (FT-IR). FT-IR spectra were recorded on a Bio-Rad Excalibur series FTS 3000 to determine the functional group. Samples were cast on a KBr disk from 2% solution and dried under vacuum.

Small- and Wide-Angle X-ray Scattering (SAXS and WAXS). SAXS and WAXS experiments were performed on beamline 17B3 of the National Synchrotron Radiation Research Center (NSRRC), Taiwan. Samples were first cast into a 1 mm thick washer, and the solvent was evaporated slowly for several days. Samples were then placed between two Kapton sheets and annealed under a nitrogen atmosphere at 200 °C for 3 days.

Transmission Electron Microscopy (TEM). Samples for TEM were prepared by slowly evaporating from 1 wt % solution for several days, followed by annealing the sample under a nitrogen environment at 200 °C for 3 days. The samples were then microtomed to form 100 nm slices and stained by exposure to the vapor of a 0.5% RuO_4 solution for 30 min. The RuO_4 preferentially stained the PPV nanodomains and enhanced the contrast between the domains. TEM images were taken with a JEOL 1230 microscope operated at an accelerating voltage of 100 kV.

Differential Scanning Calorimetry (DSC). A TA Instruments 2910 DSC was used to probe thermal transitions of polymers. Samples were prepared by solution casting directly into DSC pans and then allowing the solvent to evaporate slowly. The samples were self-assembled by heating to 200 °C and annealing for 3 days prior to DSC analysis. During DSC analysis samples were reheated to 250 °C at a rate of 5 °C/min.

Polarized Optical Microscopy (POM). A Zeiss Axiophot microscope equipped with cross-polarizers, a digital camera (Canon PowerShot A640), and a Mettler FP82HF optical hot stage connected to a Mettler FP90 controller was used to image samples. Samples were pressed between glass slides, and the experiment was performed in a nitrogen environment. The samples were heated to 220 °C with slight pressure until completely melted. The samples were then cooled and reheated at a rate of 0.2 °C/min to determine the temperature at which birefringence disappeared.

Results and Discussion

Synthesis of DEH-PPV-*b*-PMMA Rod−Coil Block Copolymer. Although the synthesis of DEH-PPV-*b*-PMMA has been demonstrated both via living free radical polymerization using a DEH-PPV macroiniatior[62−65] and end-coupling using the DEH-PPV with aldehyde end-functionality with a living polymer anion,[20,22,60] both of these techniques are limited by the chemical stability of PPV in the first case and low yields due to the nucleophilic strength of the PMMA anion in the second. Thus, we have used high reactivity and high yield "click" chemistry to synthesize DEH-PPV-*b*-PMMA.

The azido-terminated PMMA (**2**) was synthesized in two steps according to Scheme 1. The synthesis of bromine-terminated PMMA (**1**) was carried out using a ligated anionic polymerization of methyl methacrylate in the presence of LiCl,[66] followed by adding poly(methyl methacrylate) anion into a solution containing the excess amount of electrophilic coupling agent, α,α′-dibromo-*p*-xylene. The coupling agent is chosen for its high coupling efficiency.[67] GPC traces show that the obtained polymers have well-defined molecular weights and narrow polydispersities (<1.10 based on a polystyrene standards). The sharpness of the GPC traces is maintained during the addition of the bromine end-function. The degree of polymerization obtained by comparing the methylene protons (δ 4.45 ppm) neighboring the bromine end group to that from the methyl ester protons (δ 3.42−3.74 ppm) of the PMMA repeat units (Figure 1a) in ^{1}H NMR is in agreement with the molecular weight determined by GPC. The bromine end-function (**1**) was transformed into an azido functionality (**2**) via nucleophilic substitution. ^{1}H NMR spectra, as shown in Figure 1, demonstrate that the methylene protons (δ 4.45 ppm) neighboring the bromine end-group completely disappeared, and a new methylene protons (δ 4.29 ppm) adjacent to the azido group appeared. The presence of a new signal in FTIR spectrum (2099 cm^{-1}) also demonstrates the formation of the azido group. Furthermore, the ratio of signal integration between the new methylene protons and the methyl ester protons of PMMA repeating units in ^{1}H NMR is consistent with the ratio from the initial polymer (**1**).

The alkyne-terminated DEH-PPV (**3**) was synthesized from the aldehyde-terminated DEH-PPV[22] reacting with a Grignard reagent containing an alkyne functionality, as shown in Scheme 2. The Grignard reagent was prepared

Scheme 1. Synthesis of Azido-Terminated PMMA by Coupling of Anionicaly Grown PMMA with α,α′-Dibromoxylene and Subsequent Transformation into Azido Functionality

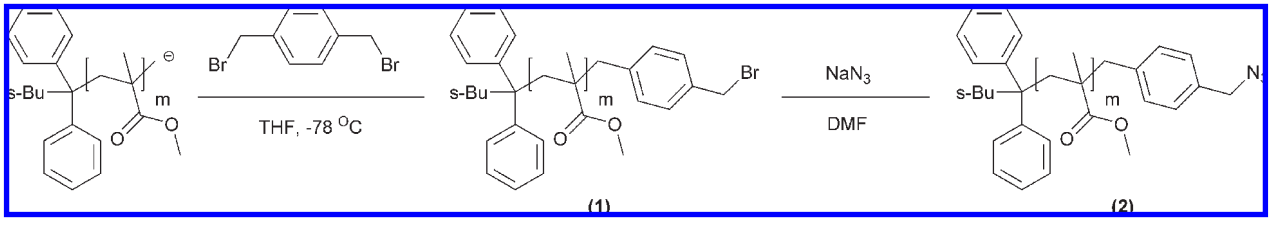

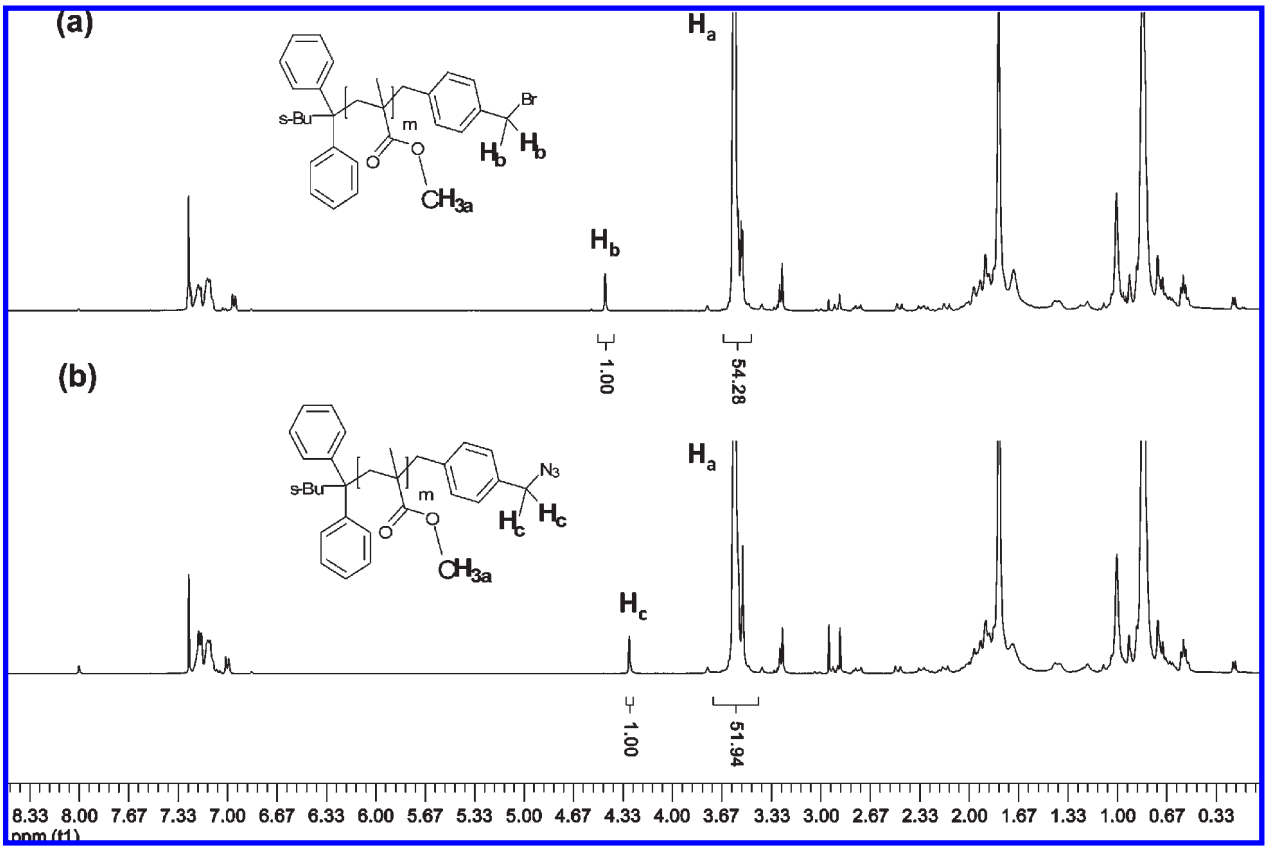

Figure 1. ^{1}H NMR spectra of the bromine- and the azido-terminated poly(methyl methacrylate)s (**1**, **2**). The degree of polymerization of **1** (a) was calculated by comparing the signal integration from the methylene protons adjacent to the bromine functionality to that from the methyl ester protons of the repeating units. The number-average molecular weight is consistent with that determined by GPC measurement. After the transformation of the bromine into azido functionality via S_N2 substitution, the methylene protons neighboring to the azido functionality appeared at upper field (b) and the original methylene protons completely disappeared. The molecular weight was also estimated from the comparison of the signal integration as above-mentioned. The results indicate the reactions are successful and efficient.

Scheme 2. Synthesis of Alkyne-Terminated PPV by Coupling of Aldehyde-Terminated PPV with Alkyne Grignard Reagent

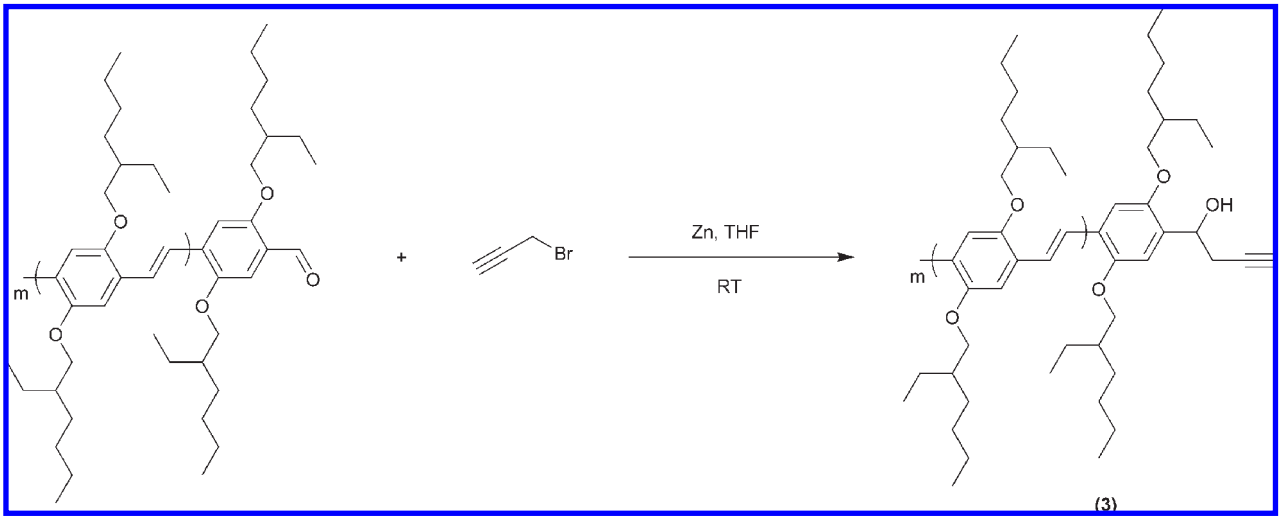

using propargyl bromide and zinc metal in THF. The alkylation of the DEH-PPV was performed with the excess amount of the Grignard reagent and carried out in moisture-free conditions. ^{1}H NMR shown in Figure 2 shows that the aldehyde proton (δ 10.47 ppm) disappeared completely, indicating high reaction yield. Moreover, the conversion was also examined by comparing the signal integration from the acetylene proton to that from the methylene protons neighboring the oxygen in the side chains of the DEH-PPV. The number-average molecular weight of the alkyne-terminated DEH-PPV remains the same as the aldehyde terminated DEH-PPV, indicating a complete conversion as well.

DEH-PPV-*b*-PMMA (**4**) rod−coil block copolymers were synthesized from the reaction of the azido-terminated PMMA and the alkyne-terminated DEH-PPV via "click" chemistry, as shown in Scheme 3. The optimized Huisgen's

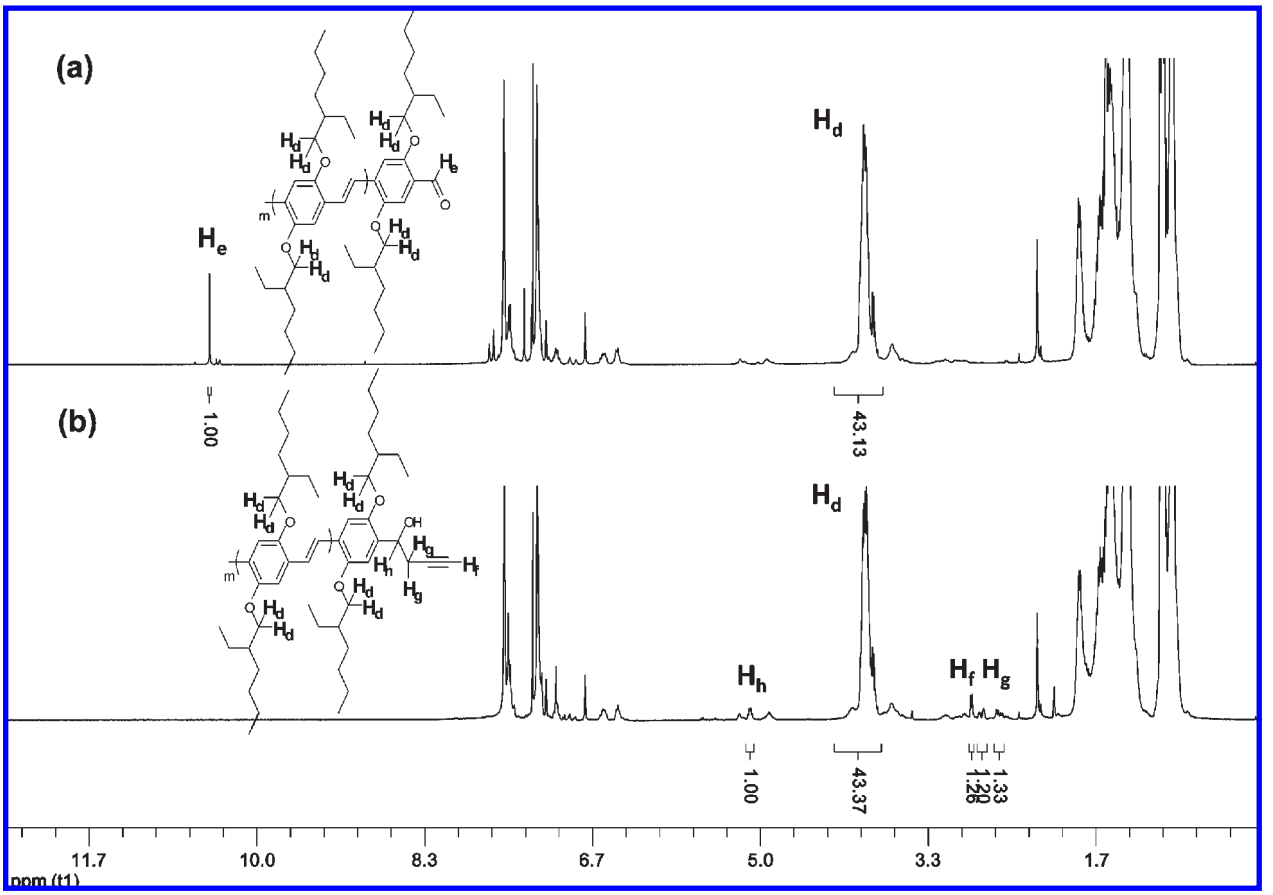

Figure 2. ^{1}H NMR spectra of aldehyde- and alkyne-terminated PPVs. The number-average molecular weight of PPV was calculated by comparing the signal integration from the aldehyde proton to that from the OCH_2 of the PPV repeating units (a). After the alkylation of the PPV, the aldehyde peak completely disappeared, and a methylene proton, an acetylene proton, and a methine proton belonging to the alkyne functionality appeared (b). The repeating units of **3** are consistent with that of the aldehyde-terminated PPV. The result indicates the alkylation is efficient by using the Grignard reagent linked to the aldehyde functionality.

Scheme 3. Synthesis of PPV-*b*-PMMA Block Copolymer via "Click" Chemistry

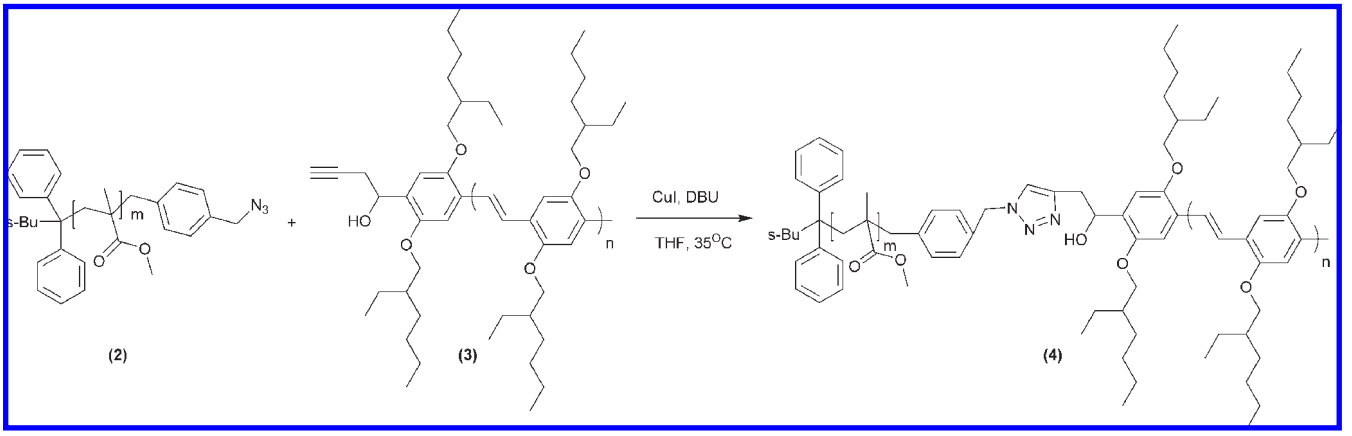

1,3-dipolar reaction was performed with CuI/DBU catalyst system in THF.[28] An excess amount of DEH-PPV (1.5 equiv) was used to ensure complete reaction of the azido-terminated PMMA. Excess DEH-PPV was easily removed by precipitation of the polymers in hexane. GPC peaks associated with the homopolymer as opposed to the block copolymer were easily distinguishable. The reaction was terminated when the intensity associated with the copolymer elution on GPC was achieved a constant value. The GPC traces of a representative polymer and its precursor are shown in Figure 3.

Morphology and Self-Assembly Behaviors. The thermodynamic behavior of rod−coil block copolymers is parametrized by four independent thermodynamic parameters in the free energy expression.[12,13] Competition between some of the above interactions also governs phase behaviors,[60,61] and the ratio between interactions creates a fifth ordering parameter.[39] As in classical block copolymer systems, the phase behavior depends on the incompatibility between the two blocks as quantified by the Flory−Huggins segregation strength, χN, and volume fraction of the constituents within the block copolymer, ϕ. Additional parameters arise

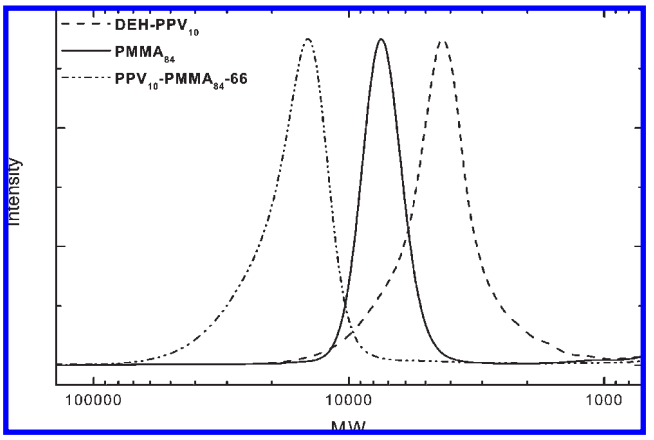

Figure 3. GPC traces of block copolymer PPV_{10}-$PMMA_{84}$-66 and its precursor polymers: DEH-PPV_{10} and $PMMA_{84}$. PPV-*b*-PMMA was synthesized by linking an azido-terminated PMMA to alkyne-terminated DEH-PPV via a "click" reaction. The increased molecular weight and low polydispersity of the block copolymer indicate the success of the optimized Huisgen's 1,3-cycloaddition reaction.

from the inherent characteristics in rod−coil block copolymers. In particular, the rod−rod interaction, μN, is used to characterize the strength of the orientational interaction favoring the alignment of the rods. Also, the volume occupied by the rod scales differently with molecular weight than the volume occupied by the coil. This difference in scaling behavior across a single chain is accounted for in terms of a geometrical asymmetry parameter (ν) which is defined as the ratio of coil radius of gyration to rod length:[12,13]

$$\nu = \frac{b\sqrt{N\phi}}{\sqrt{6}aN(1-\phi)} \quad (1)$$

where a is the statistical segment length of the rod block, b is the statistical segment length of the coil block, and N is the total number of volumetric repeat units. For the calculation of N and ϕ, the volume of a single PMMA unit is used as the reference volumetric unit, and then the number of volumetric units in the coil block would be equal to its number-average degree of polymerization. Hence, the calculation is based on the molecular weight and density of each polymer block. The molecular weight of DEH-PPV is determined using ^{1}H NMR, and the molecular weight of PMMA is measured by GPC with PMMA standards. The density of PMMA (1.19 g/cm^3) and DEH-PPV (0.988 g/cm^3) are obtained from the literature.[22,68] Furthermore, the statistical segment length of DEH-PPV, a, is defined as the length of rod that fits into the volumetric unit, calculated by the contour length of DEH-PPV over the number of volumetric units in the rod block. Using average bond lengths from the literature,[69] the contour length of DEH-PPV is 7.13 nm in this study and a is 0.162 nm. The statistical segment length of PMMA, b (0.652 nm), is estimated from previous work.[70] All molecular parameters of these block copolymers are tabulated in Table 1.

The competition between rod−rod interaction and rod−coil incompatibility is also important and can be parametrized by the rod−rod interaction over the rod−coil interaction, $G = \mu/\chi$.[13,39,61] In previously studied weakly segregated cases,[22,58,59] G was very large, and liquid crystalline interactions between the rods dominated the phase space. Sary et al. studied a case in which block segregation (χN) was much larger and as a result saw very different phases[60] Here, the value of G is intermediate such that rod−coil interactions (as opposed to liquid crystalline rod−rod interactions) are more prevalent, but phase transitions still were readily observable within SAXS and other characterization tools.

Table 1. Molecular Parameter of PPV-*b*-PMMA Block Copolymers

block copolymer	N	ϕ	ν	rod length (nm)	coil R_g (nm)	block copolymer contour length (nm)
PPV_{10}-$PMMA_{19}$-30	63	0.30	0.162	7.13	1.16	15.81
PPV_{10}-$PMMA_{36}$-43	80	0.43	0.211	7.13	1.61	23.58
PPV_{10}-$PMMA_{49}$-53	93	0.53	0.264	7.13	1.87	29.52
PPV_{10}-$PMMA_{84}$-66	128	0.66	0.347	7.13	2.44	45.51
PPV_{10}-$PMMA_{126}$-74	170	0.74	0.417	7.13	2.99	64.70

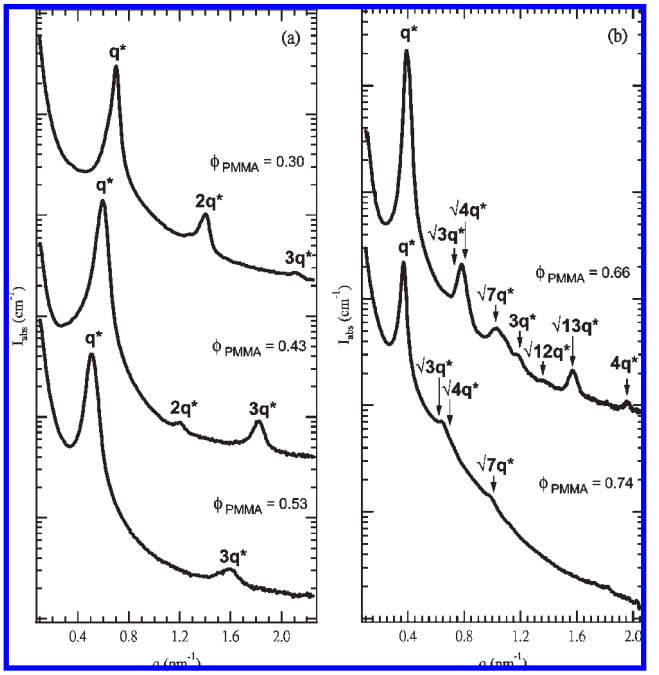

Figure 4. SAXS curves for lamellar and hexagonal morphologies in PPV-*b*-PMMA block copolymers. (a) Three block copolymers are microphase separated with peaks at integer multiples of the primary peak, indicating lamellar structure. At 53% PMMA, only the primary and the third-order peak are clearly observed due to the elimination of the lamellar structure factor peak at $2q^*$ by the form factor, suggesting symmetric spacing in lamellar phase. (b) At 66% PMMA, the polymer demonstrates long-range order hexagonal structure with peaks at q values of $\sqrt{3}q^*$, $\sqrt{4}q^*$, $\sqrt{7}q^*$, $3q^*$, $\sqrt{12}q^*$, $\sqrt{13}q^*$, and $4q^*$. At 74% PMMA, only the weak peaks at q values of $\sqrt{3}q^*$, $\sqrt{4}q^*$, and $\sqrt{7}q^*$ are observed due to the proximity of this composition to the edge of phase boundary. Curves in both graphs are offset for clarity.

The rod−coil block copolymer nanostructure is investigated in detail using small-angle X-ray scattering (SAXS) and transmission electron microscopy (TEM). The SAXS profiles for block copolymers with $\phi \leq 53\%$ are shown in Figure 4a. The polymers self-assembled into lamellar structures as indicated by peaks occurring at integer multiples of q^*. The presence of three diffraction peaks (the limit of the accessible q range on our instrumentation) indicates a highly ordered lamellar structure. While both samples of 30% and 43% coil volume fraction show three clear reflections, the $2q^*$ reflection of the sample with 53% coil volume fraction is diminished due to form factor elimination with symmetric lamellar spacing. As the coil volume fraction is increased to

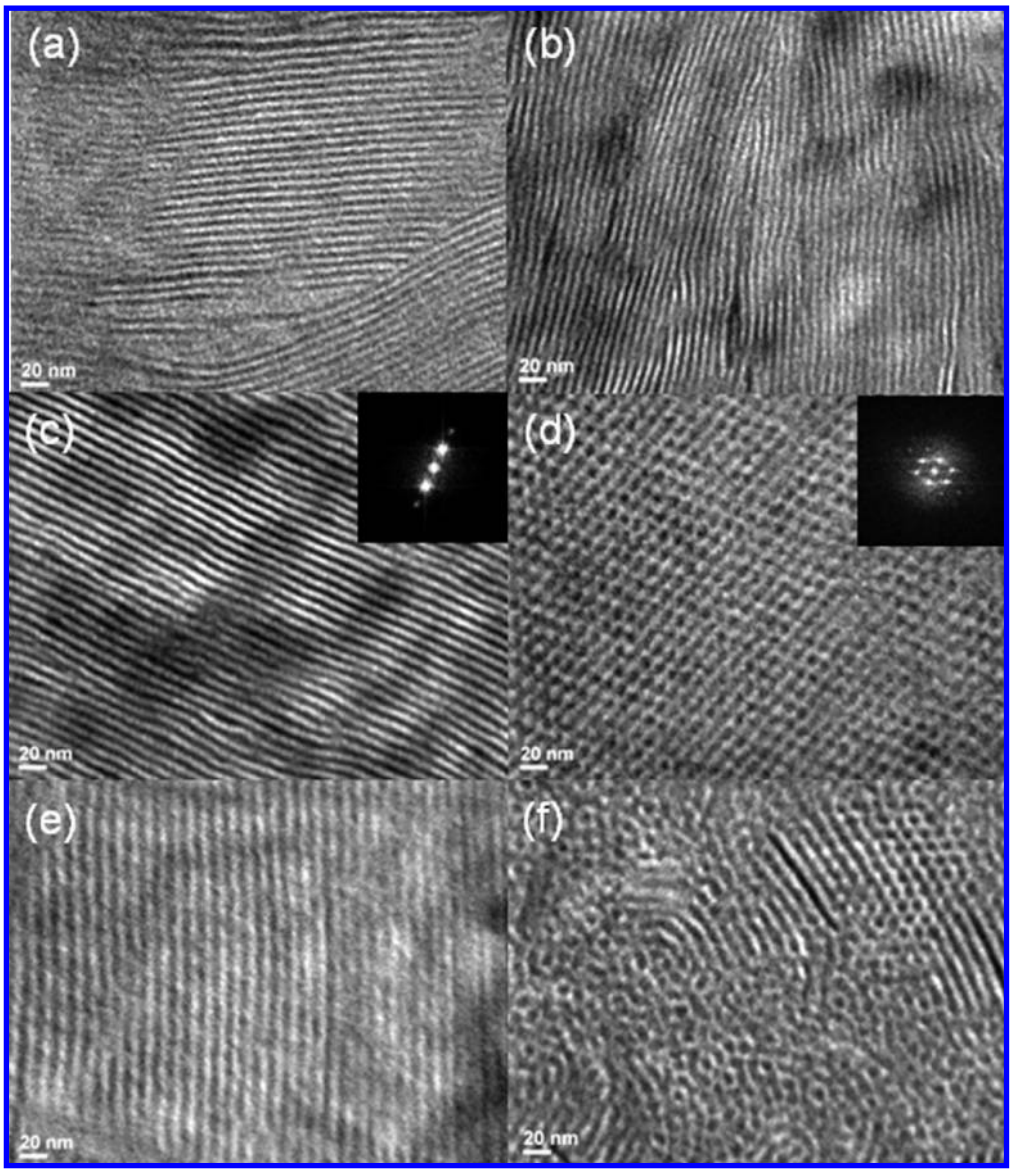

Figure 5. TEM images of PPV-*b*-PMMA block copolymers. Staining with RuO_4 reveals dark PPV nanodomains and light PMMA nanodomains in all images. The block copolymers are self-assembled into nanostructures in which only few dislocations and dilation are observed. While the coil fraction is below 53%, the block copolymers [(a) PPV_{10}-$PMMA_{13}$-30, (b) PPV_{10}-$PMMA_{36}$-43, and (c) PPV_{10}-$PMMA_{49}$-53] are self-assembled into lamellae which are extended straight for several hundred nanometers. The inset in (c) PPV_{10}-$PMMA_{49}$-53 is a 2D Fourier transformation of the polymer that has 2-fold symmetries characteristic of a lamellar structure. Hexagonally packed structures of short striplike or long striplike aggregates of the rods are observed at 66% PMMA [(d, e) PPV_{10}-$PMMA_{84}$-66]. Inset in (d) PPV_{10}-$PMMA_{84}$-66 is a 2D Fourier transform of the polymer that has 6-fold symmetries characteristic of a hexagonal structure. The lateral view of (e) PPV_{10}-$PMMA_{84}$-66 indicates striplike aggregates of the rods with one direction. Short striplike and long lying striplike aggregates with randomly direction are observed at 74% PMMA (f) due to near the edge of phase boundary.

66%, the SAXS profile shows clear high-order peaks at $\sqrt{3}q^*$, $\sqrt{4}q^*$, $\sqrt{7}q^*$, $3q^*$, $\sqrt{12}q^*$, $\sqrt{13}q^*$, and $4q^*$, indicating the rod−coil block copolymers are self-assembled into hexagonal phase in long-range order, as shown in Figure 4b. At 74% coil volume fraction, the intensity of the higher order peaks is much weaker. Only overlapping high order peaks at $\sqrt{3}q^*$ and $\sqrt{4}q^*$ and an additional peak at $\sqrt{7}q^*$ are observed. Furthermore, the structure determination from this SAXS profile is quite difficult in this case, since the reflections of the spherical and hexagonal structures are similar.

TEM provides visual information about the morphology of these lamellae. Polymers stained with RuO_4 demonstrate light PMMA-rich nanodomains and dark DEH-PPV-rich nanodomains, as shown in Figure 5. Lamellae are continuous and very long (micrometer scale in length—see Supporting Information for the TEM image of low magnification). The orientation of lamellae is correlated across several hundreds of nanometers or even up to a micrometer. Moreover, the lamellae have remarkable persistence length (at least several hundred nanometers), indicating a very high bending modulus of the DEH-PPV rod lamellar domain, as previously demonstrated.[71] The inset in Figure 5c is a 2D Fourier transformation of DEH-PPV_{10}-$PMMA_{49}$-53, demonstrating the 2-fold symmetry indicative of lamellar structure and a high degree of orientation. The defects observed in the lamellae of the DEH-PPV-*b*-PMMA system involve curvature and T junction, with only a few instances of abruptly ending lamellae (dislocations and dilations of DEH-PPV-rich regions which were previously observed in other DEH-PPV block copolymer systems).[22,58,60] We interpret this to mean that the free energy penalty associated with additional interblock contacts at the core of a dislocation

was much higher than the bending penalty imparted by the rod rigidity. As a result, this system's higher segregation strength results in greater lamellar continuity and a greater presence of curvature defects instead of lamellar breaks than previously observed.

TEM image of the more asymmetric block copolymers, as shown in Figure 5d, shows that the DEH-PPV rods are packed into short striplike aggregates assembled onto a hexagonal lattice. Moreover, the 2D Fourier transformation inset in Figure 5d has 6-fold symmetry indicative of the hexagonal structure with high degree of orientation. The lateral view of the polymer is also investigated by tilting the sample. This TEM image, as shown in Figure 5e, shows that alternating stripes with light and dark are observed. However, the stripes in the hexagonal structure are shorter than the stripes in the lamellar polymers. The short striplike aggregates with the hexagonal packing appear again, while the lamellae across the boundary (see Supporting Information for the TEM image of low magnification). In summary, in asymmetric copolymers, the DEH-PPV rods pack into hexagonally arranged strips, as previously suggested.[59,60] These strip aggregates are much longer in the third dimension than the two small dimensions. The diagonal of the hexagonal strip is evaluated as the following:

$$D = 2d\sqrt{\frac{\sqrt{3}(1-\phi)}{2\pi}} = 10.0 \text{ nm} \qquad (2)$$

where d is the lattice parameter of DEH-PPV$_{10}$-PMMA$_{84}$-66 equal to 16.34 nm. Using the rod length (Table 1) and an approximate rod diameter of 1 nm, there would be ~7 rods per short striplike aggregate.

TEM image gives complementary information for the block copolymer with coil volume fraction at 74%, as shown in Figure 5f. Short striplike aggregates and longer striplike aggregates with intermediate orientational order still can be observed. As compared to the structure of DEH-PPV$_{10}$-PMMA$_{84}$-66, the structure of DEH-PPV$_{10}$-PMMA$_{126}$-74 is similar to the hexagonal structure. The low Flory−Huggins segregation strength of this copolymer, χN, may result in both a diffuse phase boundary and decreased long-range ordering.

Recently, the presence of hexagonal structures was proposed for rod−coil copolymer with high coil fractions (>87%) and high geometric asymmetries ($\nu > 0.587$) in a system near the weak segregation limit.[59,60] Similarly, Pryamitsyn and Ganesan have shown the change of copolymer morphology are influenced by varying ν using 2D-SCFT theoretical calculation.[13] They predicted the presence of lamellar and nonlamellar structures for rod−coil copolymer by assuming an intermediate G value of 4. Reenders and ten Brinke obtained similar results at the same value of G.[39] In the present study, we observe the hexagonal structure at relatively low coil fraction (66%) and relatively low ν (0.347) as compared to the studies above. Reenders and ten Brinke have suggested the importance of competition between rod−rod interactions (μ) and rod−coil interactions (χ) in determining phase behavior. This competition parameter, G, controls the interplay between liquid crystalline ordering and microphase separation ordering. When the G value is high, the rod−rod interaction of liquid crystalline ordering will dominate, leading to only the formation of lamellar structure. This is similar to behavior experimentally observed by Olsen et al.[14,59,72] and Sary et al.[60,61] Varying G will result in the variations of boundaries between different phases and perhaps allow for a more expansive phase space than the lamellar dominated phase diagram present at high G and the low ν.

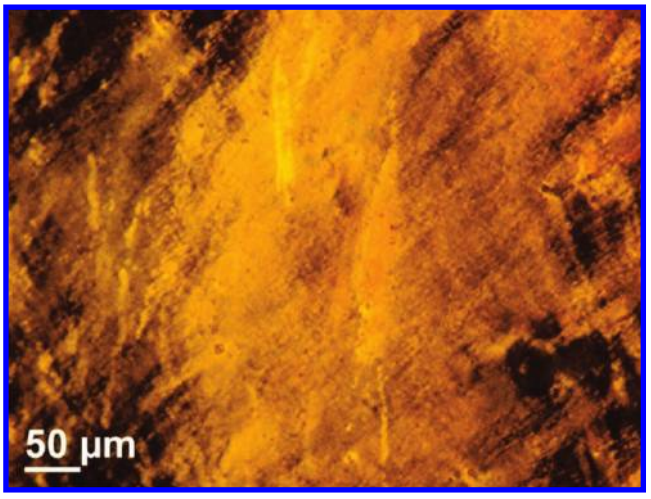

Figure 6. A birefringent smectic phase at 140 °C was observed in 66% PMMA copolymer (PPV$_{10}$-PMMA$_{84}$-66), but no grain boundaries are observed.

Table 2. Phase Transition Temperature of PPV-*b*-PMMA Copolymers (°C)

block copolymer	SI transition (POM)	SI transition (WAXS)	SI transition (DSC)	ODT
PPV$_{10}$-PMMA$_{13}$-30	187 ± 2	180 ± 10	185 ± 20	220 ± 5
PPV$_{10}$-PMMA$_{36}$-43	190 ± 3	180 ± 10	185 ± 18	200 ± 5
PPV$_{10}$-PMMA$_{49}$-53	189 ± 2	180 ± 10	185 ± 16	195 ± 5
PPV$_{10}$-PMMA$_{84}$-66	191 ± 2	180 ± 10	185 ± 15	190 ± 5
PPV$_{10}$-PMMA$_{126}$-74	193 ± 3	180 ± 10	185 ± 17	190 ± 5

Phase Transitions. The DEH-PPV-based rod−coil block copolymers may go through several transitions as microphase-separated disorders upon heating, since DEH-PPV homopolymer has transitions from crystalline to smectic and then to nematic phases.[73] We have used temperature varied polarized optical microscopy (POM) to study the phase transitions of liquid crystalline DEH-PPV in DEH-PPV-*b*-PMMA. Smectic phases with small grains are observed for lamellae forming copolymers with low coil fraction (53% PMMA). A very large grain birefringent smectic phase is observed for hexagonally ordered copolymer which has high coil fraction (66% PMMA) (Figure 6). The liquid crystalline clearing temperatures from smectic phase to isotropic phase for five different composition copolymers are determined and summarized in Table 2. The transition temperatures are in the same range with a deviation less than 6 °C between the lamellae forming copolymer and the hexagonally ordered copolymer. In the isotropic state, some small regions of birefringence were kinetically trapped in coil-rich copolymers (>66% coil fractions). As expected in kinetic trapping, the presence of these regions increased with coil fraction due to a decrease in chain mobility.

The smectic phase describes the two-dimensional stacking of the layers, but the in-plane stacking of the rods is also of interest. Wide-angle X-ray scattering (WAXS) is used to characterize the spacing of the DEH-PPV rods on the molecular level, as shown in Figure 7. The large peak at ~6.5 nm^{-1} is observed in all polymers and corresponds to lateral rod−rod spacing, indicating that the packing mechanisms of the DEH-PPV rods in the lamellar phase

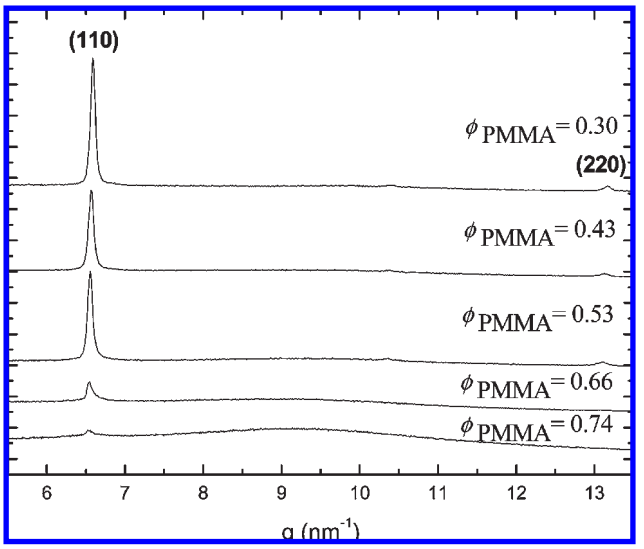

Figure 7. WAXS curves for PPV-*b*-PMMA block copolymers. The primary peak around 6.5 nm^{-1} corresponds to the rod−rod spacing in all polymers indicative of same packing mechanism.

and the hexagonal phase are the same. Further, the rod−rod spacing is similar to that previously reported for DEH-PPV homopolymers (6.5 nm^{-1}).[73] Figure 8 shows the evolution of WAXS patterns as a function of temperature for two polymers with lamellar structure and hexagonal structure. The peak intensity remains the same upon heating to 170 °C; upon further heating, the intensity starts to decay gradually, suggesting the continuous disruption of packed rods. The peak disappears around 180−190 °C indicative of the complete disruption of the rod−rod packing. The results of five copolymers with different compositions are given in Table 2. The liquid crystalline transition temperatures of copolymers observed by WAXS are in the same range obtained by POM. Furthermore, the rod−rod spacing as a function of temperature for five copolymers is plotted in Figure 9. The slight increase in rod−rod spacing of all copolymers through a range from ambient temperature to 190 °C corresponds to a change in intermolecular spacing. The change is less than 0.1 nm which is attributed to the thermal expansion upon heating.

Differential scanning calorimetry (DSC) was also used to study the phase transitions upon heating (see Supporting Information). A similar transition for five copolymers is observed, and the results are listed in Table 2. The transition starts from 165 °C and ends around 200 °C, indicating a broad transition range. The results are in qualitative agreement with the results from POM and WAXS.

To understand the segregation strength of the block copolymers, SAXS experiments with varying temperature were performed. As the block copolymers were heated, these polymers went through a transition from an ordered structure to a microphase disordered state. The SAXS intensity plots of two representative polymers—one is lamellar structure (53% volume fraction of PMMA) and the other is hexagonal structure (66% volume fraction of PMMA)—are shown in Figure 10. The microphase order−disorder transition temperature (ODT) is characterized by the disappearance of higher order peaks in the SAXS profiles and an abrupt drop in intensity of the primary scattering peak with increasing temperature. To find the divergence of primary peak intensity, the transition temperature also can be quantified through discontinuities in a plot of inverse intensity of primary peak versus inverse temperature, as shown in Figure 11. The temperature of the divergence of

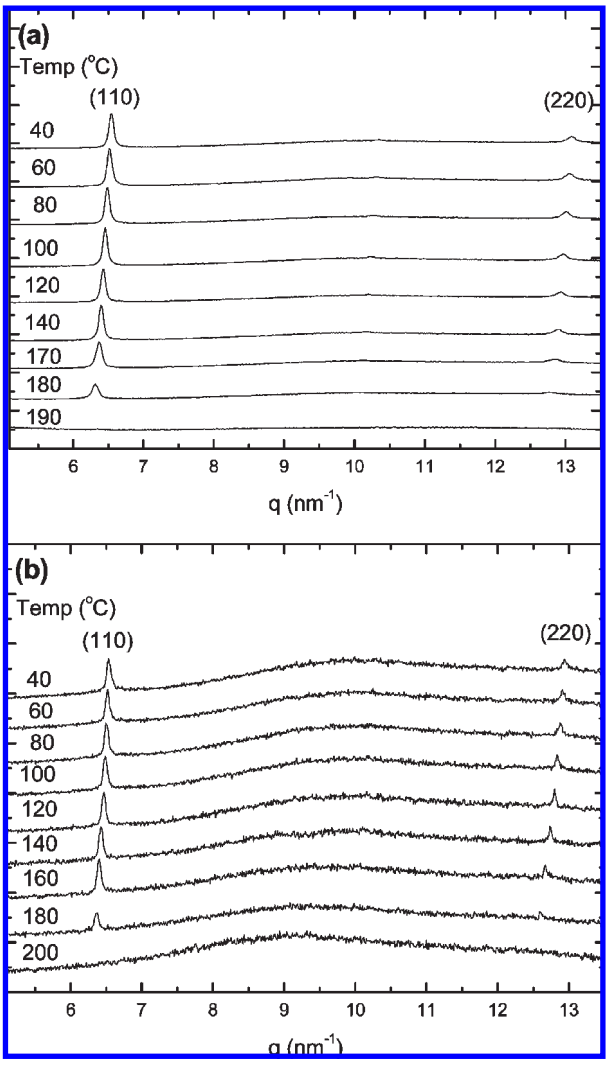

Figure 8. WAXS curves for PPV-*b*-PMMA block copolymers at different temperatures. (a) PPV_{10}-$PMMA_{49}$-53 shows the primary peak around 6.55 nm^{-1} corresponds to the spacing between the rod blocks in lamellar structure. The intensity of the peak remains constant until approaching the T_{SI}, and the peak completely disappears before the ODT. (b) PPV_{10}-$PMMA_{84}$-66 shows the primary peak around 6.54 nm^{-1} corresponds to the spacing between the rod blocks in hexagonal structure. The intensity of the peak remains constant until the temperature is near the T_{SI} and the ODT. Curves in both graphs are offset for clarity.

primary peak intensity is found at the same temperature as the disappearance of higher order peaks. The ODT of five different copolymers are tabulated in Table 2. The ODT steadily decreases with increasing coil fraction, and the tendency of ODT change is qualitatively consistent with theoretical predictive.[13,39,40,42,43] As compared with the POM, DSC, and WAXS studies, the ODT is higher than the SI transition for the copolymer with lamellar structure, but the ODT is in the same range as the SI transition for the hexagonally ordered copolymer. Because the well-aligned DEH-PPV rods are restricted in the nanodomain, even though the copolymers lose their long-range order slight above the ODT (>66%, still in phase separation status as shown in Figure 10), there is barely extra spatial space to extend the DEH-PPV rods with the same direction and form the nematic phase. As the results indicate, there is no nematic phase transition present in the copolymers.

Except for the liquid crystalline transition in the ordered phase as above-mentioned, the DEH-PPV-*b*-PMMA

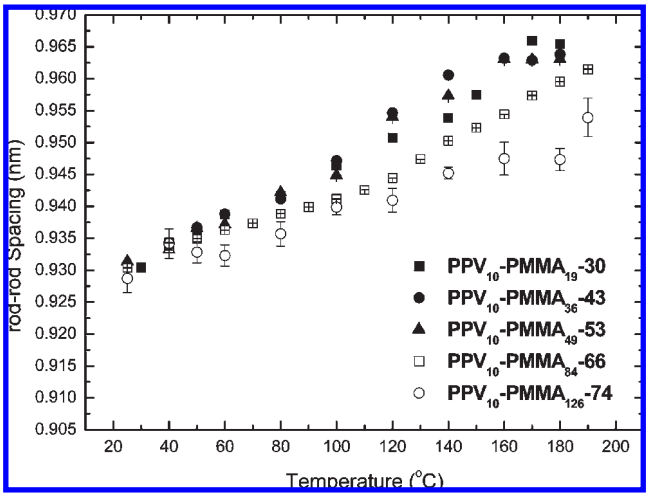

Figure 9. Lateral rod−rod spacing as a function of temperature for PPV-*b*-PMMA block copolymers. In all polymers, the rod−rod spacing slightly increases with increasing temperature due to the thermal expansion.

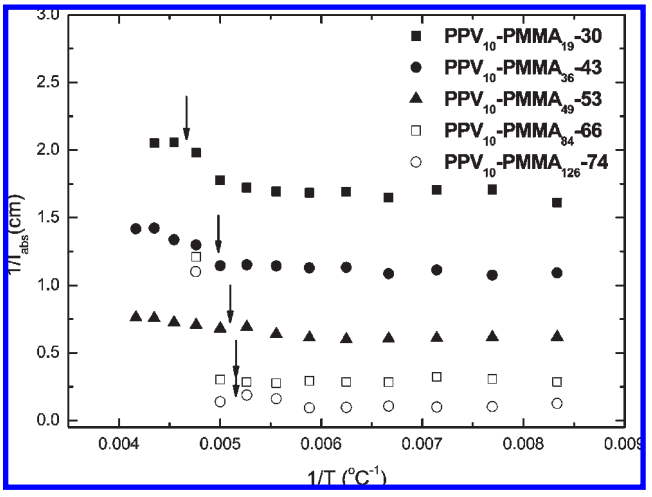

Figure 11. Inverse SAXS intensity in the vicinity of the order−disorder transition (ODT). The discontinuity in the slope of the intensity vs inverse temperature curve indicates the order−disorder transition.

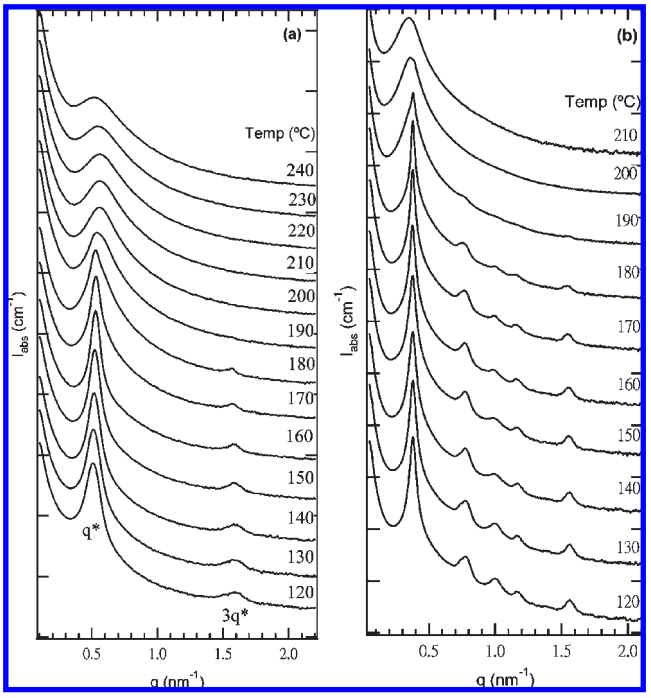

Figure 10. SAXS curves for PPV-*b*-PMMA block copolymers in the vicinity of order−disorder transition. (a) At 53% PMMA (PPV_{10}-$PMMA_{49}$-53), only the primary and the third-order peak observed indicate the equal domain spacing of a lamellar structure. Higher order peaks disappear above 190 °C, indicating the order−disorder transition. (b) At 66% PMMA (PPV_{10}-$PMMA_{84}$-66), the polymer demonstrates the hexagonal phase of high long-range order with peaks at q values of $\sqrt{3}q^*$, $\sqrt{4}q^*$, $\sqrt{7}q^*$, $3q^*$, $\sqrt{12}q^*$, $\sqrt{13}q^*$, and $4q^*$. Higher order peaks disappear above 190 °C, indicating the order−disorder transition. Curves in both graphs are offset for clarity.

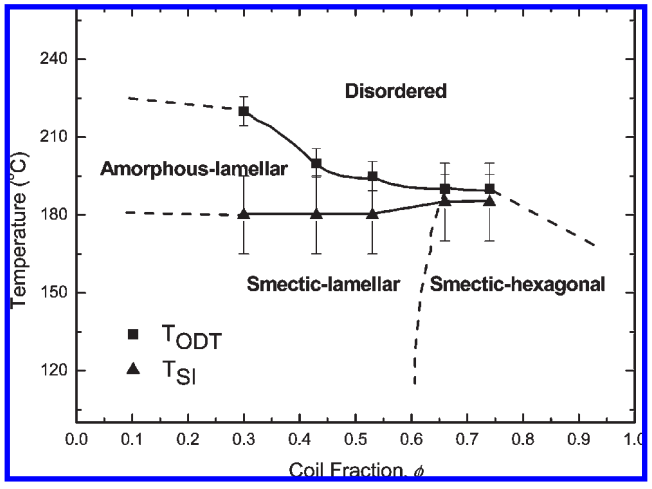

Figure 12. Phase diagram for PPV-*b*-PMMA block copolymers. The rod block length was held constant for all copolymers synthesized while coil length was varied. For coil fractions below 53%, polymers transition is from a disordered to amorphous−lamellar to smectic−lamellar structure upon cooling. For coil fraction above 66%, polymers transition is from a disordered to smectic−hexagonal packed structure upon cooling. The phase diagram is in qualitative agreement with intermediate G rod−coil copolymer predicted by the calculations based on Landau expansions and 2D self-consistent-field theory (2D SCFT).

rod−coil block copolymers may also have several transitions upon heating, resulting from a competition between rod-and-coil interfacial tension and stretching of the coils. The arrangements of rods and coils with varying temperature may reflect on the change of domain spacing. In rod−coil block copolymers, the lamellar phase and hexagonal phase may consist of several rod arrangements such as monolayers, bilayers, etc. Theoretical predictions suggest bilayer arrangements of rods are favored in rod-rich regimes with strong segregation.[12,13,36−38] Comparing the domain spacing from TEM images (Figure 5) and SAXS profiles (Figure 4) with the molecular parameters (Table 1) of the block copolymers, the results suggest the rods are organized in either monolayers or in greatly tilted bilayers. Furthermore, there is no discontinuous variation in domain spacing observed in SAXS upon heating and no characteristic transition in DSC that might indicate a change from bilayers to monolayers. We can speculate the rods pack into lamellar and hexagonally symmetric phases composed smectic monolayer due to the intermediate segregation in our DEH-PPV-*b*-PMMA system.

Phase Diagram of DEH-PPV-*b*-PMMA. Through the data analysis of accumulated results obtained from SAXS, WAXS, TEM, POM, and DSC, a phase diagram for intermediate G and intermediately segregated rod−coil block copolymers is established, as shown in Figure 12. When the temperature is low, the rods tend to align into smectic

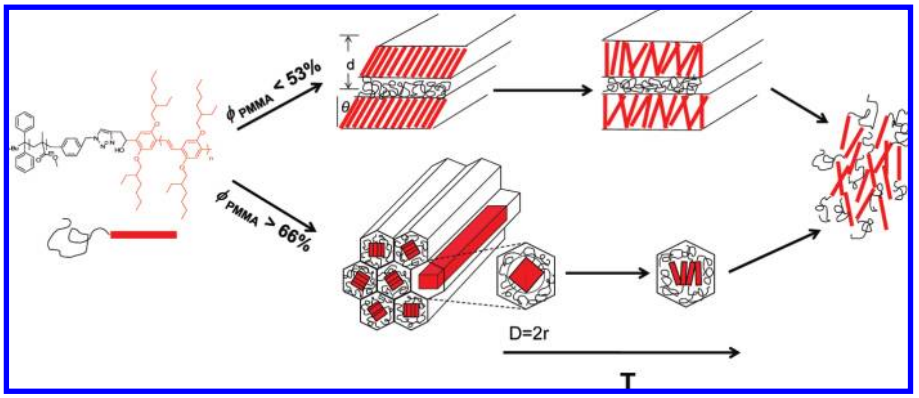

Figure 13. Schematic illustrations of possible rod segment packing in PPV-*b*-PMMA rod−coil block copolymers. From above to below, lamellar structure and hexagonal structure are shown, respectively. While the coil fraction is lower than 53%, the rods aggregate into lamellae with tilted angle. Upon heating, the rods disrupt within the lamellar nanodomain since T_{SI} is below ODT. At higher coil fraction, the rods are organized into hexagonal structure with ~7 rods per nanodomain striplike aggregates. The results have been confirmed by SAXS profiles and TEM images.

layers while the rods and coils separate from each other forming smectic−lamellar structures at low coil fractions (ϕ < 53%) and smectic−hexagonal structures at higher coil fractions (ϕ > 66%). With increasing temperature, the well-packed rods in the smectic ordered phase are disrupted and eventually become an isotropically disordered phase as sketched in Figure 13. The T_{SI} of copolymers with different coil fractions remains similar and is consistent with homo-DEH-PPV and is generally lower than or at the same temperature as the block copolymer microphase order−disorder temperature (ODT). This result suggests that the rods may lose their smectic character while still confined within a lamellar or striplike nanodomain forming an amorphous−lamellar phase. As observed through DSC and WAXS, the melting transition of the rods within a nanodomain is broad and gradual. With increasing coil fraction, the microphase ODT decreases toward the T_{SI}, resulting in a decreased presence of the amorphous−lamellar phase. Within the striplike hexagonal structure, the smectic−isotropic transition is higher in temperature presumably due to confinement effects, and as a result the rods appear to disorder simultaneously with the disordering of the block copolymer nanodomains.

The transition from smectic−lamellar to amorphous−lamellar to disorder is in agreement with predictions by Reenders and ten Brinke.[39] Their calculations also predict a significant influence of *G* in shifting the phase boundaries and the sequential order of transitions. As the *G* decreases, the Flory−Huggins (rod−coil segregation) interaction will dominate, and in the limit of no liquid crystalline interactions (*G* approaching 0), the phase diagram at lower coil fractions will be analogous to the phase diagram of a classical coil−coil block copolymer. Whereas, the Maier−Saupe (rod−rod) interaction will dominate at very large *G*, resulting in only lamellar phase present in a broad range of coil fractions. Our observation of a hexagonal phase appears to be in-line with the predictions at lower *G*. We do not observe an expected body-centered-cubic phase, which presumably would appear at even higher coil fractions in an even more segregated regime.[60] Our experimental results are also in agreement with SCFT predictions. Matsen and Barett as well as [12] Pryamitsyn and Ganesan[13] predicted that the smectic phase of monolayer can be observed in lamellar structures at intermediate segregation strengths. Changes in the coil fraction and the relative block size would also induce transitions in smectic phases, leading to the changes in domain size. 2D-SCFT calculations[13,42] also qualitatively predict that a nonlamellar structure can be observed in coil-rich regimes in addition to the presence of lamellar structure in rod-rich regimes. The strip or puck structure predicted by Pryamitsyn and Ganesan is experimentally observed as the hexagonal strips of DEH-PPV-*b*-PMMA copolymer in coil-rich regimes. The phase diagram of the DEH-PPV-*b*-PMMA system is successfully compared with the intermediate *G* strength system predicted by using Landau expansion theory and self-consistent-field theory (SCFT). It is very important to note that the *G* has a great influence on the phase behavior. The *G* is mainly controlled by the chemical structures of copolymers since the definition of the *G* is the rod−rod interaction over the rod−coil interaction. Evaluation of *G* may be useful in evaluating and unifying the broad range of rod−coil block copolymer behavior present in the literature.

Conclusions

A series of DEH-PPV-*b*-PMMA rod−coil bock copolymers with narrow polydispersity (PDI < 1.1) were prepared successfully using "click" chemistry. The alkyne-terminated DEH-PPV and the azido-terminated PMMA were synthesized with high yield and then were end-coupled with high yield. The polymers were characterized using ^{1}H NMR and GPC measurements, and the results show the reactions were successful in each step. The results of SAXS, TEM, POM, DSC, and WAXS reveal that the copolymers exhibit intermediate segregation strength and can be self-assembled into smectic−lamellar structures with low coil fraction (< 53%) and into smectic−hexagonal structures with higher coil fractions (> 66%). Upon heating, the smectic−isotropic transition and order−disorder transition were observed for low coil fraction copolymers. However, the smectic−isotropic transition occurred simultaneously with the order−disorder transition for high coil fraction copolymer. The T_{SI} of copolymer remains the same as the homo-DEH-PPV regardless its coil fraction, indicating that the segregation between rod and coil was strong enough to allow the rod to be unaffected by the presence of a microdomain boundary. A phase diagram has constructed for this copolymer system which is in qualitative agreement with predictions from Landau expansion theory[39] and 2D-SCFT[13] for an intermediate *G* factor of rod−coil copolymer.

Acknowledgment. We gratefully acknowledge the financial support from the National Science Council of Taiwan (NSC 95-3114-P-002-003-MY3). Work at UC Berkeley/Lawrence Berkeley National Laboratories was supported by the DOE-BES Plastic Electronics Program at Lawrence Berkeley National Laboratories. We also thank the Department of Chemistry of National Taiwan University for the use of its NMR spectrometer. We gratefully acknowledge Dr. U-Ser Jeng and Dr. Chiu-Hun Su

for help with SAXS/WAXS experiments at the National Synchrotron Radiation Research Center, Taiwan.

Supporting Information Available: TEM images of DEH-PPV-*b*-PMMA block copolymers at lower magnification and DSC thermograms of DEH-PPV and DEH-PPV-*b*-PMMA block copolymers. This material is available free of charge via the Internet at http://pubs.acs.org.

References and Notes

(1) Bates, F. S. *Science* **1991**, *251* (4996), 898–905.
(2) Bates, F. S.; Fredrickson, G. H. *Phys. Today* **1999**, *52* (2), 32–38.
(3) Park, C.; Yoon, J.; Thomas, E. L. *Polymer* **2003**, *44* (22), 6725–6760.
(4) Olsen, B. D.; Segalman, R. A. *Mater. Sci. Eng., R* **2008**, *62* (2), 37–66.
(5) de Boer, B.; Stalmach, U.; van Hutten, P. F.; Melzer, C.; Krasnikov, V. V.; Hadziioannou, G. *Polymer* **2001**, *42* (21), 9097–9109.
(6) Hulvat, J. F.; Sofos, M.; Tajima, K.; Stupp, S. I. *J. Am. Chem. Soc.* **2005**, *127* (1), 366–372.
(7) Lin, H. C.; Lee, K. W.; Tsai, C. M.; Wei, K. H. *Macromolecules* **2006**, *39* (11), 3808–3816.
(8) Lu, S.; Liu, T. X.; Ke, L.; Ma, D. G.; Chua, S. J.; Huang, W. *Macromolecules* **2005**, *38* (20), 8494–8502.
(9) Sivula, K.; Ball, Z. T.; Watanabe, N.; Frechet, J. M. *J. Adv. Mater.* **2006**, *18* (2), 206–210.
(10) Yu, W. L.; Meng, H.; Pei, J.; Huang, W.; Li, Y. F.; Heeger, A. J. *Macromolecules* **1998**, *31* (15), 4838–4844.
(11) Sary, N.; Rubatat, L.; Brochon, C.; Hadziioannou, G.; Mezzenga, R. *Macromol. Symp.* **2008**, *268*, 28–32.
(12) Matsen, M. W.; Barrett, C. *J. Chem. Phys.* **1998**, *109* (10), 4108–4118.
(13) Pryamitsyn, V.; Ganesan, V. *J. Chem. Phys.* **2004**, *120* (12), 5824–5838.
(14) Olsen, B. D.; Shah, M.; Ganesan, V.; Segalman, R. A. *Macromolecules* **2008**, *41* (18), 6809–6817.
(15) Liu, J. S.; Sheina, E.; Kowalewski, T.; McCullough, R. D. *Angew. Chem., Int. Ed.* **2002**, *41* (2), 329–332.
(16) Iovu, M. C.; Jeffries-El, M.; Sheina, E. E.; Cooper, J. R.; McCullough, R. D. *Polymer* **2005**, *46* (19), 8582–8586.
(17) Van De Wetering, K.; Brochon, C.; Ngov, C.; Hadziioannou, G. *Macromolecules* **2006**, *39* (13), 4289–4297.
(18) Dai, C. A.; Yen, W. C.; Lee, Y. H.; Ho, C. C.; Su, W. F. *J. Am. Chem. Soc.* **2007**, *129* (36), 11036–11038.
(19) Boudouris, B. W.; Frisbie, C. D.; Hillmyer, M. A. *Macromolecules* **2008**, *41* (1), 67–75.
(20) Li, W. J.; Wang, H. B.; Yu, L. P.; Morkved, T. L.; Jaeger, H. M. *Macromolecules* **1999**, *32* (9), 3034–3044.
(21) Wang, H. B.; Wang, H. H.; Urban, V. S.; Littrell, K. C.; Thiyagarajan, P.; Yu, L. P. *J. Am. Chem. Soc.* **2000**, *122* (29), 6855–6861.
(22) Olsen, B. D.; Segalman, R. A. *Macromolecules* **2005**, *38* (24), 10127–10137.
(23) Urien, M.; Erothu, H.; Cloutet, E.; Hiorns, R. C.; Vignau, L.; Cramail, H. *Macromolecules* **2008**, *41* (19), 7033–7040.
(24) Ho, C. C.; Dai, C. A.; Su, W. F. *J. Appl. Polym. Sci.* **2009**, *111* (3), 1571–1580.
(25) Kolb, H. C.; Finn, M. G.; Sharpless, K. B. *Angew. Chem., Int. Ed.* **2001**, *40* (11), 2004–2021.
(26) Tornoe, C. W.; Christensen, C.; Meldal, M. *J. Org. Chem.* **2002**, *67* (9), 3057–3064.
(27) Kolb, H. C.; Sharpless, K. B. *Drug Discovery Today* **2003**, *8* (24), 1128–1137.
(28) Opsteen, J. A.; van Hest, J. C. M. *Chem. Commun.* **2005**, No. 1, 57–59.
(29) Agut, W.; Taton, D.; Lecommandoux, S. *Macromolecules* **2007**, *40* (16), 5653–5661.
(30) Binder, W. H.; Sachsenhofer, R. *Macromol. Rapid Commun.* **2007**, *28* (1), 15–54.
(31) Li, H. Y.; Riva, R.; Jerome, R.; Lecomte, P. *Macromolecules* **2007**, *40* (4), 824–831.
(32) Tao, Y.; Ma, B.; Segalman, R. A. *Macromolecules* **2008**, *41* (19), 7152–7159.
(33) Lutz, J. F. *Angew. Chem., Int. Ed.* **2007**, *46* (7), 1018–1025.
(34) Halperin, A. *Europhys. Lett.* **1989**, *10* (6), 549–553.
(35) Halperin, A. *Macromolecules* **1990**, *23* (10), 2724–2731.
(36) Semenov, A. N. *Mol. Cryst. Liq. Cryst.* **1991**, *209*, 191–199.
(37) Semenov, A. N.; Vasilenko, S. V. *Zh. Eksp. Teor. Fiz.* **1986**, *90* (1), 124–140.
(38) Williams, D. R. M.; Fredrickson, G. H. *Macromolecules* **1992**, *25* (13), 3561–3568.
(39) Reenders, M.; ten Brinke, G. *Macromolecules* **2002**, *35* (8), 3266–3280.
(40) Holyst, R.; Schick, M. *J. Chem. Phys.* **1992**, *96* (1), 730–740.
(41) Singh, C.; Goulian, M.; Liu, A. J.; Fredrickson, G. H. *Macromolecules* **1994**, *27* (11), 2974–2986.
(42) Li, W.; Gersappe, D. *Macromolecules* **2001**, *34* (19), 6783–6789.
(43) Muller, M.; Schick, M. *Macromolecules* **1996**, *29* (27), 8900–8903.
(44) Netz, P. R.; Schick, M. *Phys. Rev. Lett.* **1996**, *77* (2), 302–305.
(45) Babin, J.; Taton, D.; Brinkmann, M.; Lecommandoux, S. *Macromolecules* **2008**, *41* (4), 1384–1392.
(46) Klok, H. A.; Langenwalter, J. F.; Lecommandoux, S. *Macromolecules* **2000**, *33* (21), 7819–7826.
(47) Lecommandoux, S.; Achard, M. F.; Langenwalter, J. F.; Klok, H. A. *Macromolecules* **2001**, *34* (26), 9100–9111.
(48) Minich, E. A.; Nowak, A. P.; Deming, T. J.; Pochan, D. J. *Polymer* **2004**, *45* (6), 1951–1957.
(49) Chen, J. T.; Thomas, E. L.; Ober, C. K.; Mao, G. P. *Science* **1996**, *273* (5273), 343–346.
(50) Li, C. Y.; Tenneti, K. K.; Zhang, D.; Zhang, H. L.; Wan, X. H.; Chen, E. Q.; Zhou, Q. F.; Carlos, A. O.; Igos, S.; Hsiao, B. S. *Macromolecules* **2004**, *37* (8), 2854–2860.
(51) Tenneti, K. K.; Chen, X. F.; Li, C. Y.; Tu, Y. F.; Wan, X. H.; Zhou, Q. F.; Sics, I.; Hsiao, B. S. *J. Am. Chem. Soc.* **2005**, *127* (44), 15481–15490.
(52) Lee, M.; Cho, B. K.; Kim, H.; Yoon, J. Y.; Zin, W. C. *J. Am. Chem. Soc.* **1998**, *120* (36), 9168–9179.
(53) Lee, M.; Cho, B. K.; Kim, H.; Zin, W. C. *Angew. Chem., Int. Ed.* **1998**, *37* (5), 638–640.
(54) Lee, M.; Cho, B. K.; Zin, W. C. *Chem. Rev.* **2001**, *101* (12), 3869–3892.
(55) Radzilowski, L. H.; Carragher, B. O.; Stupp, S. I. *Macromolecules* **1997**, *30* (7), 2110–2119.
(56) Radzilowski, L. H.; Stupp, S. I. *Macromolecules* **1994**, *27* (26), 7747–7753.
(57) Ryu, J. H.; Oh, N. K.; Zin, W. C.; Lee, M. *J. Am. Chem. Soc.* **2004**, *126* (11), 3551–3558.
(58) Olsen, B. D.; Segalman, R. A. *Macromolecules* **2006**, *39* (20), 7078–7083.
(59) Olsen, B. D.; Segalman, R. A. *Macromolecules* **2007**, *40* (19), 6922–6929.
(60) Sary, N.; Rubatat, L.; Brochon, C.; Hadziioannou, G.; Ruokolainen, J.; Mezzenga, R. *Macromolecules* **2007**, *40* (19), 6990–6997.
(61) Sary, N.; Brochon, C.; Hadziioannou, G.; Mezzenga, R. *Eur. Phys. J. E* **2007**, *24* (4), 379–384.
(62) van der Veen, M. H.; de Boer, B.; Stalmach, U.; van de Wetering, K. I.; Hadziioannou, G. *Macromolecules* **2004**, *37* (10), 3673–3684.
(63) Sary, N.; Mezzenga, R.; Brochon, C.; Hadziioannou, G.; Ruokolainen, J. *Macromolecules* **2007**, *40* (9), 3277–3286.
(64) Qu, G.; Jiang, F. F.; Zhang, S. Y.; Usuda, S. J. *Mater. Lett.* **2007**, *61* (16), 3421–3424.
(65) Brochon, C.; Sary, N.; Mezzenga, R.; Ngov, C.; Richard, F.; May, M.; Hadziioannou, G. *J. Appl. Polym. Sci.* **2008**, *110* (6), 3664–3670.
(66) Varshney, S. K.; Jacobs, C.; Hautekeer, J. P.; Bayard, P.; Jerome, R.; Fayt, R.; Teyssie, P. *Macromolecules* **1991**, *24* (18), 4997–5000.
(67) Scriven, E. F. V.; Turnbull, K. *Chem. Rev.* **1988**, *88* (2), 297–368.
(68) Shetter, J. A. *J. Polym. Sci., Part B: Polym. Lett.* **1963**, *1* (5), 209–213.
(69) Allen, F. H.; Kennard, O.; Watson, D. G.; Brammer, L.; Orpen, A. G.; Taylor, R. *J. Chem. Soc., Perkin Trans. 2* **1987**, No. 12, S1–S19.
(70) Fetters, L. J.; Lohse, D. J.; Richter, D.; Witten, T. A.; Zirkel, A. *Macromolecules* **1994**, *27* (17), 4639–4647.
(71) Olsen, B. D.; Alcazar, D.; Krikorian, V.; Toney, M. F.; Thomas, E. L.; Segalman, R. A. *Macromolecules* **2008**, *41* (1), 58–66.
(72) Olsen, B. D.; Segalman, R. A. *Macromolecules* **2005**, *38* (24), 10127–10137.
(73) Olsen, B. D.; Jang, S. Y.; Luning, J. M.; Segalman, R. A. *Macromolecules* **2006**, *39* (13), 4469–4479.